Thermal Stability of Complex Oxide Combustion Catalyst Supports

Marcus F. M. Zwinkels,† Stéphanie Druesne, P. Govind Menon, Emilia Björnbom, and Sven G. Järås*

Department of Chemical Engineering and Technology-Chemical Technology, Kungl Tekniska Högskolan (Royal Institute of Technology), S-100 44 Stockholm, Sweden

As part of a search for more thermostable supports for combustion catalysts for gas turbine applications, a series of complex oxide materials were prepared by sol−gel synthesis and two different coprecipitation routes. The materials were chosen on the basis of literature studies; two hexaaluminates ($LaAl_{11}O_{18}$ and $BaMnAl_{11}O_{19-\alpha}$), a perovskite ($SrZrO_3$), a spinel ($MgAl_2O_4$), and a pyrochlore ($La_2Zr_2O_7$). After synthesis, the materials were aged for 16 h in a flow of humid air at temperatures between 1100 and 1400 °C, simulating the actual conditions in a catalytic combustor. The aged samples were characterized by X-ray diffraction, nitrogen adsorption for determination of BET surface area, and scanning electron microscopy. The sol−gel materials generally exhibited higher thermal stability than their coprecipitated counterparts. One exception was $LaAl_{11}O_{18}$, which had the highest surface area of all materials, 8 m^2/g, after aging at 1400 °C, both for the sol−gel synthesized and one coprecipitated material. The reaction paths for the high-temperature solid-state reactions depended on preparation procedure and stoichiometry of the product.

Introduction

Catalytic fuel combustion is recognized as a promising technology for decreasing NO_x emissions from gas turbines (Kolaczkowski, 1995; Zwinkels *et al.*, 1993; Zwinkels, 1996). Placing a catalyst in a gas turbine combustor implies severe demands on the properties of the catalyst. Among the most important properties are high combustion activity at typical combustor inlet conditions, i.e., 300−400 °C, thermal stability at temperatures between 1000 and 1400 °C, and high thermal shock resistance (Prasad *et al.*, 1984). High activity is favored by a high catalyst surface area (Arai *et al.*, 1986; Zwinkels *et al.*, 1995). The activity and stability requirements are usually in conflict (McCarty and Wise, 1990), and hence engineering solutions have been proposed to circumvent the contradiction between activity and stability, such as a hybrid combustor (Furuya *et al.*, 1987), a partial catalytic combustor (Dalla Betta *et al.*, 1994), and a multimonolith combustor (Sadamori *et al.*, 1994). The first two combustor concepts limit the catalyst temperature by converting only part of the fuel over the catalyst and the remainder in a homogeneous downstream combustion zone. The multimonolith combustor is based on a segmented catalyst, allowing the catalyst stability and activity to be tailored for different positions in the combustor. The highest thermal stability is obviously required for the hot zone near the combustor outlet.

Various promising thermostable materials have been reported in the literature. A series of hexaaluminate materials were developed by Arai and coworkers (Machida *et al.*, 1987, 1989). Their sol−gel synthesized barium hexaaluminate ($BaAl_{12}O_{19}$) exhibited high thermal stability at temperatures over 1400 °C. They incorporated manganese in the hexaaluminate lattice, creating catalytic activity (Machida *et al.*, 1989) while maintaining high thermal stability. Groppi *et al.* (1993) recently achieved similar performance when preparing the manganese-substituted barium hexaaluminate using coprecipitation. Lowe *et al.* (1995) prepared various complex oxide gel powders, of which lanthanum hexaaluminate ($LaAl_{11}O_{18}$) showed the highest thermal stability. Alumina-containing spinels with Zn (Marion *et al.*, 1991) and Mg, Ni, and Co (Marti *et al.*, 1994) were also reported to be interesting. Another class of thermostable materials are perovskites, e.g., $LaAlO_3$ (Lowe *et al.*, 1995; Johansson *et al.*, 1996; Marti *et al.*, 1995) and $SrZrO_3$ (Lowe *et al.*, 1995). Pyrochlores ($A_2B_2O_7$) exhibit high chemical stability at high temperatures (Ashcroft *et al.*, 1989), and their use as combustion catalysts was recently suggested (Ramesh *et al.*, 1994).

Judging from the recent literature, various promising materials for high-temperature catalytic combustion exist. However, the thermal stability and in particular the surface area stability may be improved significantly. Moreover, many studies involve aging of materials in stagnant air for only a few hours. It is well-known that steam, inevitably present in a combustor, strongly enhances sintering of porous materials (Trimm, 1991).

In the present study, we report the thermal stability of a series of promising materials in humid flowing air at temperatures between 1100 and 1400 °C. The following materials were chosen for this study: two hexaaluminate materials ($LaAl_{11}O_{18}$ and $BaMnAl_{11}O_{19-\alpha}$), a perovskite ($SrZrO_3$), a spinel ($MgAl_2O_4$), and a pyrochlore ($La_2Zr_2O_7$). These materials were prepared using sol−gel synthesis and coprecipitation in order to study the effect of the preparation procedure on the properties of the product. Sol−gel synthesis was chosen since it may yield highly porous and very homogeneous mixed oxides (Brinker and Scherer, 1990). Coprecipitation, on the other hand, has the advantage of less expensive raw materials that can be handled more easily.

* Corresponding author. E-mail: svenj@ket.kth.se. Tel.: +46 8 790 8917. Fax: +46 8 108 579.

† Current address: AB Sandvik Coromant, Lerkrogsvägen 19, S-126 80 Stockholm, Sweden.

S0888-5885(96)00421-6 CCC: $15.00
Published on Web 02/02/1998

Table 1. Summary of the Prepared Materials with Preparation Routes, Calculated Hydrolysis Ratios for the Sol−Gel Syntheses, and Calculated and Measured Cation Ratios for the Products

material ID	target composition	prep. route	hydrol ratio	molar cation ratio		comments
				calc	meas	
LA-SG	$LaAl_{11}O_{18}$	SG	2.5	1:11.0	1:12.9	supercrit drying
LA-CP1	$LaAl_{11}O_{18}$	CP-1		1:11.0	1:11.9	rapid NH_3 addition
LA-CP2	$LaAl_{11}O_{18}$	CP-2		1:11.0	1:11.8	
MA-SG	$MgAl_2O_4$	SG	3	1:2.00	1:2.66	supercrit drying
MA-CP1	$MgAl_2O_4$	CP-1		1:3.45	1:3.77	
MA-CP2	$MgAl_2O_4$	CP-2		1:2.00	1:1.93	
BMA-SG	$BaMnAl_{11}O_{19-\alpha}$	SG	1.87	1:1.00:11:0		supercrit drying
BMA-CP	$BaMnAl_{11}O_{19-\alpha}$	CP-1		1:1.00:11.0		
SZ-SG1	$SrZrO_3$	SG	20	1:1.00	1:1.14	supercrit drying
SZ-SG2	$SrZrO_3$	SG	20	1:1.04	1:0.92	ambient drying
SZ-CP	$SrZrO_3$	CP-1		1:0.86	1:17.3	
LZ-SG	$La_2Zr_2O_7$	SG	6	1:1.00	1:2.94	ambient drying
LZ-CP	$La_2Zr_2O_7$	CP-2		1:1.00	1:0.81	

Experimental Section

Synthesis and Materials. The sol−gel route (SG) was based on the hydrolysis of metal alkoxides. Suitable amounts of reactants were dissolved in 2-propanol. In all cases, one of the metals was provided as a metal alkoxide, whereas the other was added as an inorganic salt. Two metal salts were used in the case of the Ba−Mn hexaaluminate. After hydrolysis, the formed gel was aged overnight at room temperature and washed three times with 2-propanol before drying and calcination. The product was either dried under supercritical conditions or at room temperature. Supercritical drying was done in a 250 mL stainless steel autoclave (Haage Apparaten). After the sample was placed in the autoclave, the system was pressurized to 2 MPa with nitrogen. The subsequent increase in temperature to about 300 °C caused a further rise in pressure to 7−8 MPa. The solvent was vented at this high temperature, after which the system was cooled. The dried product was calcined at 500 and 1000 °C consecutively for 4 h each.

Two different approaches for coprecipitation were followed.

Route 1 (CP1): Ammonia was added to an acidic aqueous mixture of metal salts, thereby slowly increasing the pH, which led to the precipitation of a mixed hydroxide.

Route 2 (CP2): An aqueous metal salt mixture was added dropwise to a solution with a pH kept constant at 8.5, using ammonia. Each drop immediately precipitated once in contact with the basic solution.

After precipitation, the product was aged overnight at room temperature and washed three times with deionized water. The washed product was dried at 200 °C and then calcined at 500 and 1000 °C consecutively for 4 h each.

A summary of the materials prepared and synthesis routes followed is given in Table 1. The starting chemicals used in the syntheses of the complex oxides listed in Table 1 were aluminum nitrate nonahydrate (Aldrich, >98%), aluminum isopropoxide (Johnson Matthey, >98%), barium nitrate (Aldrich, >99%), lanthanum nitrate hexahydrate (Merck, >99%), magnesium nitrate hexahydrate (Johnson Matthey, >99%), manganese nitrate hexahydrate (Aldrich, >98%), anhydrous strontium nitrate (Johnson Matthey, >99%), zirconium oxynitrate (Aldrich, >99%), and zirconium *n*-propoxide (70 wt % solution in *n*-propanol, Johnson Matthey).

A commercial boehmite (Pural SCF 55, Condea Chemie GmbH) with a surface area of 253 m^2/g was calcined and aged in the same way as the prepared mixed oxides in order to serve as a reference.

Table 1 also gives the hydrolysis ratios in the sol−gel syntheses, defined as moles of water per mole of metal alkoxide. The obtained molar cation ratios in the products were determined using inductive coupled plasma atomic spectroscopy (ARL 3520 B ICP analyzer). These ratios can be compared with the values calculated from the used amounts of starting chemicals, also given in Table 1.

Aging and Characterization. Aging experiments were performed with materials calcined at 1000 °C. Samples were aged in tubular furnaces with aluminosilicate (1100−1200 °C) or dense alumina (1300−1400 °C) tubes. Dense alumina boat-shaped crucibles were used in all experiments. All samples were aged for 16 h at one temperature in flowing air containing approximately 10 vol % steam.

The phase compositions of the calcined and aged samples were investigated by powder X-ray diffraction using a Siemens Diffraktometer 5000 operating with the following parameters: Cu Kα radiation, 30 mA, 40 kV, Ni filter, 2θ scanning range 10−85°, and scan step size 0.02. The BET surface area and pore volume were determined by nitrogen adsorption using a Micromeritics ASAP 2000. Samples were outgassed in vacuum at 250 °C for at least 3 h before the adsorption measurements. The microstructure of the samples was investigated by scanning electron microscopy (SEM) using a Zeiss DSM 940.

Results and Discussion

In this section, the obtained results are presented and discussed. These results mainly comprise surface area stability data and XRD patterns. The former is the most common way to represent thermal stability of combustion catalysts, whereas XRD data give indications on the crystal structure of the material during various stages of preparation and thermal treatment. The formation of crystalline phases is normally closely related to crystal growth and hence loss of surface area and is thus an important aspect in aging studies.

$LaAl_{11}O_{18}$. Three different lanthanum hexaaluminate samples were prepared: LA-SG by sol−gel and LA-CP1 and LA-CP2 by the coprecipitation routes 1 and 2, respectively. The surface areas of the three materials are given for different aging temperatures in Figure 1, also showing the surface area of the commercial boehmite-based Al_2O_3 as reference.

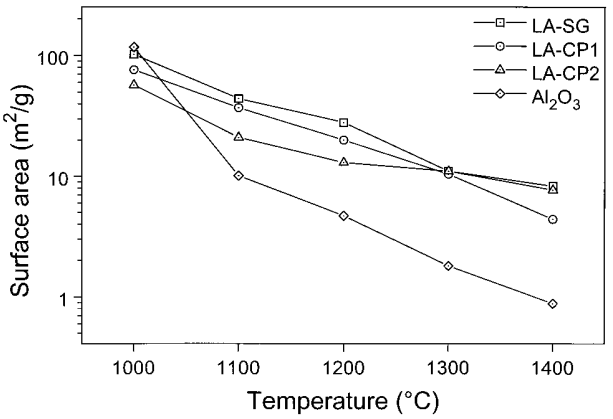

Figure 1. Surface areas for the $LaAl_{11}O_{18}$ samples and a commercial Al_2O_3 after aging in a 10% H_2O in air flow for 16 h at various temperatures. The figures for 1000 °C represent the surface areas after calcination in stagnant dry air.

Figure 1 shows that all lanthanum hexaaluminate samples had superior thermal stability compared to the commercial Al_2O_3. The highest stability was exhibited by the sol−gel sample, having 8.2 m^2/g after aging at 1400 °C. The surface area−aging temperature relations for the coprecipitated samples show some interesting features. The LA-CP1 sample follows the sol−gel sample fairly well up to 1300 °C, after which its surface area drops rapidly. The LA-CP2 sample had a lower area than the other two lanthanum hexaaluminate samples after calcination and after aging to 1200 °C. However, at higher temperatures, the decrease in surface area for the LA-CP2 sample was less than for the other two samples. As a result, LA-CP2 and LA-SG had nearly the same surface areas after aging at 1300 and 1400 °C. The observed surface areas for LA-SG at different temperatures agree well with literature data (Lowe *et al.*, 1995). The surface area of LA-CP1 (20 m^2/g) at 1200 °C is similar to the value reported by Kato *et al.* (Kato *et al.*, 1988) (23.6 m^2/g) for a material with a La:Al ratio of about 1:10, prepared by a similar coprecipitation method. Kato *et al.* showed that the surface area strongly depended on the La:Al ratio. The surface area of the LA-CP2 sample (13 m^2/g) after 1200 °C is lower than the 51.3 m^2/g reported by Marti *et al.* (1995). This difference may partly be due to the presence of water during aging and the longer aging time in our case. The use of acetone by Marti *et al.* in the final washing step might also have been advantageous. Perhaps it would be beneficial for the surface area of the product if the synthesis were performed in a nonaqueous solvent.

The X-ray diffraction patterns of two of the three $LaAl_{11}O_{18}$ samples are given in Figure 2. A similar development of the target $LaAl_{11}O_{18}$ phase can be observed for these materials, as well as for the LA-CP1 sample. At 1000 °C, the materials are very amorphous, with a trace of δ-Al_2O_3 in the case of the coprecipitation samples and a trace of $LaAlO_3$ for the sol−gel sample. After aging at 1100 °C, the perovskite $LaAlO_3$ appears with sharp peaks. The intensities of the $LaAlO_3$ peaks increase with aging temperature up to 1300 °C, where a maximum is reached. The intensities then decrease after aging at 1400 °C. The target $LaAl_{11}O_{18}$ phase starts to appear after aging at 1100 °C and the intensities of the peaks of this phase continuously increase with aging temperature up to 1400 °C, the highest temperature studied.

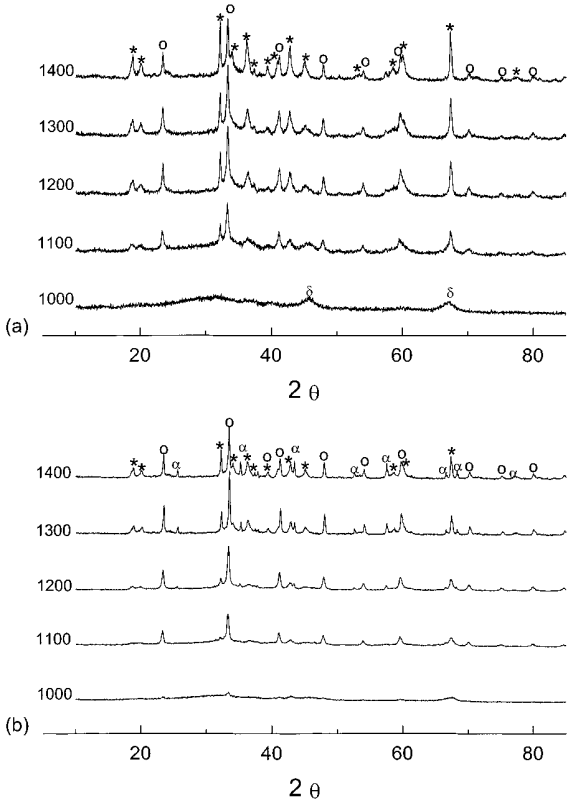

Figure 2. X-ray diffraction patterns of LA-CP2 (a) and LA-SG (b) after aging at different temperatures (°C). Peak intensities in arbitrary units. Key: (★) $LaAl_{11}O_{18}$; (○) $LaAlO_3$; (δ) δ-Al_2O_3; (α) α-Al_2O_3.

The commercial Al_2O_3 appeared as a mixture of δ- and θ-Al_2O_3 after calcination at 1000 °C, the sample being rather amorphous. However, already after 1100 °C, the α-phase prevailed in the Al_2O_3 sample, which then had become very crystalline. At still higher temperatures, the peaks for α-Al_2O_3 became higher and sharper, indicating extensive growth of the crystals, accompanied by a severe loss of surface area.

Various interesting observations can be made when the diffraction patterns of the lanthanum aluminate samples at increasing temperatures are compared. The first is the fact that the peak intensities for LA-SG are much higher than for the coprecipitated samples, indicating a much higher degree of crystallinity. The second observation is the high relative intensity of the $LaAlO_3$ peaks in the sol−gel sample compared to the coprecipitated samples. The third observation is the presence of small α-Al_2O_3 peaks in the LA-CP1 and LA-SG patterns.

The relative intensities of the phases present in the samples appear to depend on the composition of the product as well as the preparation method. This observation agrees with literature data. Lowe *et al.* (1995) observed both $LaAlO_3$ and $LaAl_{11}O_{18}$ phases in the case of a lanthanum-rich mixed complex oxide (Al/La < 11), whereas $LaAl_{11}O_{18}$ and α-Al_2O_3 were observed for the aluminum-rich complex oxide, both prepared by sol−gel synthesis. Similar observations were made by Kato *et al.* for a coprecipitated lanthanum aluminate (Kato *et al.*, 1988). The three samples in this study all had an excess of aluminum, which in two of three cases gave rise to the formation of some α-Al_2O_3.

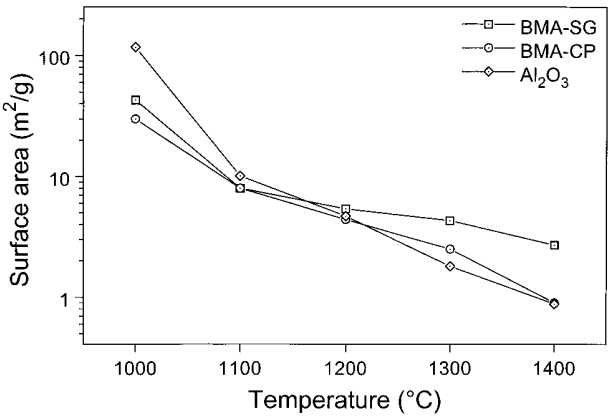

Figure 3. Surface areas for the $BaMnAl_{11}O_{19-\alpha}$ samples after aging in a 10% H_2O in air flow for 16 h at various temperatures. The figures for 1000 °C represent the surface areas after calcination in stagnant dry air.

It is now widely accepted that the thermal stability of $LaAl_{11}O_{18}$ and other hexaaluminate materials, such as $BaAl_{12}O_{19}$, is related to the nonisotropic growth of the crystals, yielding a high-aspect-ratio crystalline material (Machida *et al.*, 1988; Groppi *et al.*, 1995). SEM confirmed the presence of platelike structures in all three lanthanum aluminate samples.

However, the mechanism of formation of the hexaaluminate or β-alumina phase appears to depend on the preparation procedure used. $BaAl_{12}O_{19}$ prepared from a mixture of alkoxides appeared directly from an amorphous mixed oxide precursor (Machida *et al.*, 1988). On the other hand, when prepared by coprecipitation (Groppi *et al.*, 1995), or when barium acetate was used in the sol−gel synthesis (Lowe *et al.*, 1995), $BaAl_2O_4$ was observed as an intermediate phase, assumed to react with transition aluminas to form the final $BaAl_{12}O_{19}$. Similar to the latter mechanism, we observed the $LaAlO_3$ phase as an intermediate in the formation of $LaAl_{11}O_{18}$, both for the sol−gel sample and the coprecipitated materials. The form of both cations in the precursor solution apparently influences the mixed hydroxide formed, and hence the prevailing mechanism for the solid-state conversion to the final phase.

$BaMnAl_{11}O_{19-\alpha}$. Two manganese-substituted barium hexaaluminate samples were prepared. Figure 3 shows the surface areas of the coprecipitation (BMA-CP) and the sol−gel (BMA-SG) sample after aging at various temperatures. Again, the surface area of the commercial alumina is included for comparison.

The surface areas for BMA-CP and BMA-SG after aging at 1300 °C are about half of the values reported by Machida *et al.* (1989) for an alkoxide-based material and by Groppi *et al.* (1993) for a coprecipitated material. Again, the presence of steam during aging in our case is likely to be one reason for the observed discrepancy in measured surface areas. Another reason may be the slight differences in preparation procedures. The use of barium nitrate instead of the barium isopropoxide used by Machida *et al.* in the sol−gel synthesis is one of them. Our BMA-CP sample was prepared by coprecipitation route 1, whereas the method followed by Groppi *et al.* was very similar to our route 2.

The observations made with X-ray diffraction, shown in Figure 4, are in line with the above discussion on the formation of the hexaaluminate phase in lanthanum aluminum and barium aluminum mixed oxides. Both

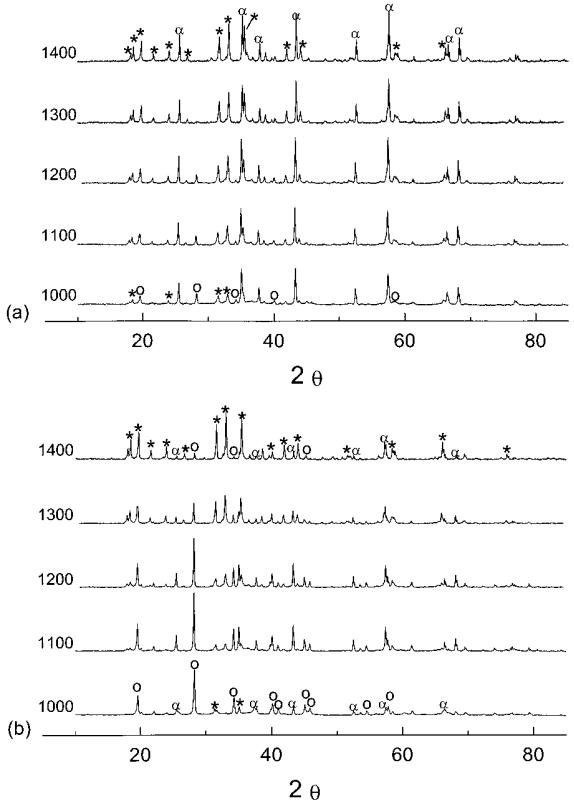

Figure 4. X-ray diffraction patterns of BMA-CP (a) and BMA-SG (b) after aging at different temperatures (°C). Peak intensities in arbitrary units. Key: (★) $BaMnAl_{11}O_{19-\alpha}$; (○) $BaAl_2O_4$; (α) α-Al_2O_3.

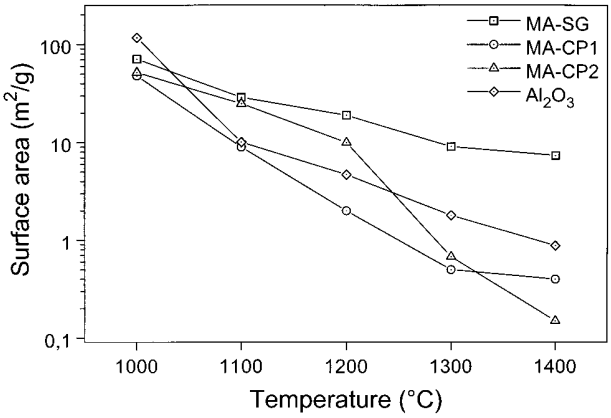

Figure 5. Surface areas for the $MgAl_2O_4$ samples after aging in a 10% H_2O in air flow for 16 h at various temperatures. The figures for 1000 °C represent the surface areas after calcination in stagnant dry air.

the BMA-CP and BMA-SG samples show rather poor crystallinity at 1000 °C, with $BaAl_2O_4$ and α-Al_2O_3 as prevailing phases. The intensity of the $BaAl_2O_4$ peaks decreases at higher aging temperatures with concomitant formation of the hexaaluminate phase. The sol−gel sample only exhibits traces of α-Al_2O_3 once the hexaaluminate is formed, whereas α-Al_2O_3 is much more prominent in the coprecipitated sample.

$MgAl_2O_4$. Three magnesium aluminate samples were prepared, one by sol−gel synthesis, MA-SG, and two by coprecipitation following the two routes described above, MA-CP1 and MA-CP2. Figure 5 shows the surface areas of the three samples after aging at various

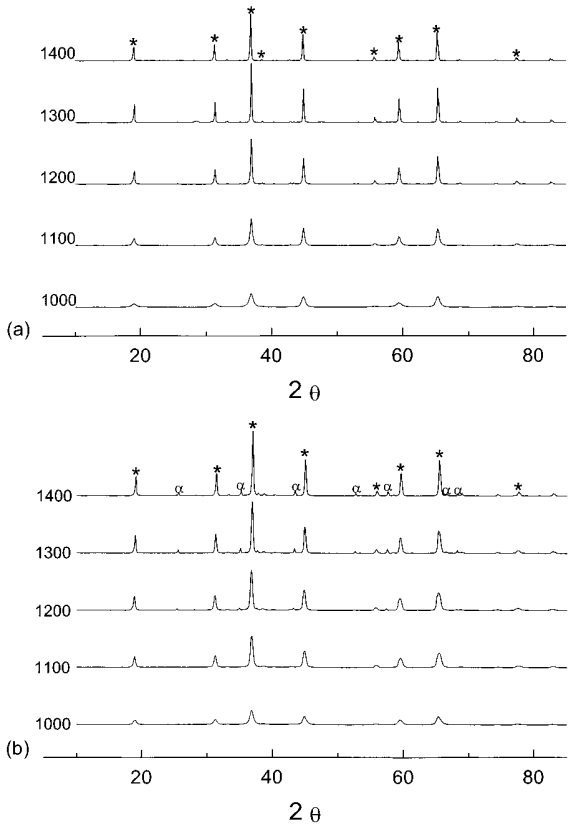

Figure 6. X-ray diffraction patterns of MA-CP2 (a) and MA-SG (b) after aging at different temperatures (°C). Peak intensities in arbitrary units. Key: (★) $MgAl_2O_4$; (α) α-Al_2O_3.

temperatures and a comparison of these materials with the commercial alumina.

Clearly, the sol−gel sample exhibits excellent thermal stability compared to the two coprecipitated materials. The material prepared by route 2 is nearly as good as the gel up to 1100 °C, but the surface area drops rapidly at higher temperatures. The material prepared by coprecipitation route 1 has a much lower surface area than the gel under all conditions. The phase compositions of the materials, derived from the X-ray diffraction patterns, shown in Figure 6, offer no real explanation for this difference in thermal stability. The sol−gel material is very homogeneous and shows only traces of α-Al_2O_3 at 1400 °C. The diffraction patterns of two coprecipitated materials reveal certain differences. The material prepared by route 1 exhibits sharp α-Al_2O_3 from 1100 °C and up, whereas the material prepared by route 2 (Figure 6a) is monophasic at all temperatures. Table 1 shows that both MA-CP1 and MA-SG contain more aluminum than required for the target phase, 89 and 33%, respectively. On the other hand the molar ratio of MA-CP2 is very close to the desired value. The composition of the magnesium aluminate appears to be a dominant parameter for the phase purity, more than the preparation method.

However, the preparation method clearly has a strong effect on the surface area stability of the magnesium aluminate spinel. The $MgAl_2O_4$ gel, though it contains α-Al_2O_3 impurities, has a better thermal stability than the coprecipitated sample, prepared by route 2.

It has been proposed that a high porosity could render high thermal stability (Lowe *et al.*, 1995). This appears not to be the reason for the observed differences in

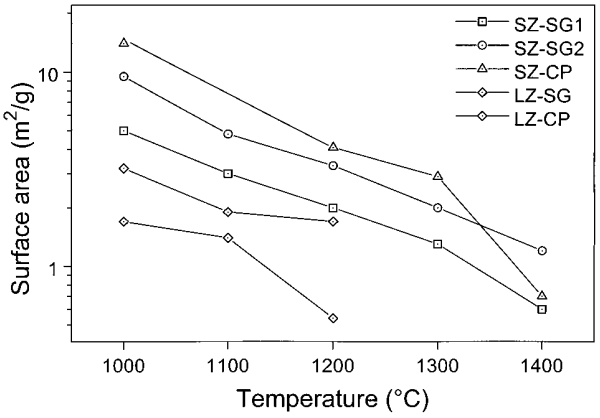

Figure 7. Surface areas for the $SrZrO_3$ and $La_2Zr_2O_7$ samples after aging in a 10% H_2O in air flow for 16 h at various temperatures. The figures for 1000 °C represent the surface areas after calcination in stagnant dry air.

thermal stability for the $MgAl_2O_4$ samples in our case. MA-CP2 had a higher pore volume than MA-SG up to 1200 °C, after which it dropped as dramatically as the surface area. The pore volume of MA-SG exhibited a much more gradual decrease with increasing temperature. The higher surface area stability of MA-SG compared to MA-CP2 may be related to differences in morphology. For samples aged at 1200 °C and higher, the spinel-related peaks in the diffraction pattern of MA-SG are much broader than for MA-CP2, indicating a much smaller crystallite size for the former. Scanning electron microscopy confirmed this interpretation. Large well-ordered cubic crystallites were observed in case of the coprecipitated sample, whereas much smaller irregular particles were seen in the gel.

The thermal stability observed for MA-SG was higher than reported by Lowe *et al.* (1995) for a $MgAl_2O_4$ gel. Their material was of similar composition and also showed traces of α-Al_2O_3. The surface area of MA-CP2 at 1200 °C (10 m^2/g) was lower than the 43 m^2/g reported by Marti *et al.* (1994), but they calcined their material in dry air for 8 h.

$SrZrO_3$. Two sol−gel samples were prepared, one dried under supercritical conditions (SZ-SG1) and the other dried at ambient conditions (SZ-SG2), in addition to one coprecipitation sample, following route 1 (SZ-CP). Figure 7 shows the surface areas of these three samples after aging at various temperatures.

Generally, the surface areas were low for the three samples, also compared to literature data (Lowe *et al.*, 1995). Unlike the hexaaluminates discussed above, whose two-dimensional or nonisotropic structure hinders sintering, the perovskite structure of $SrZrO_3$ allows sintering in three dimensions, yielding a material with a low aspect ratio and low surface area.

The phases observed in the $SrZrO_3$ samples after aging at various temperatures are summarized in Table 2. All samples are highly crystalline already at 1000 °C. The sol−gel sample, dried under supercritical conditions, was nearly monophasic, with a trace of monoclinic zirconia at the highest aging temperatures. The sample dried at ambient conditions showed a very similar diffraction pattern, with slightly higher amounts of monoclinic zirconia. The coprecipitation sample on the other hand is very heterogeneous, and the desired phase is not obtained. Instead, the prevailing phase is monoclinic zirconia.

Table 2. Crystalline Phases Observed in the Sr and La Zirconates after Calcination in Air (1000 °C) and Aging at Various Temperatures in a 10 vol % H_2O in Air Flow for 16 h (Major Phases in Bold Print)[a]

material	target composition	temp (°C) 1000	1100	1200	1300	1400
SZ-SG1	$SrZrO_3$	**SZ**, TZ	**SZ**	**SZ**	**SZ**	**SZ**, MZ(T)
SZ-SG2	$SrZrO_3$	**SZ**, TZ	**SZ**	**SZ**, MZ	**SZ**, MZ	**SZ**, MZ
SZ-CP	$SrZrO_3$	**TZ**, MZ	**MZ**, TZ, SZ	**MZ**, SZ	**MZ**, SZ	**MZ**, SZ
LZ-SG	$La_2Zr_2O_7$	**TZ**	**LZ**, TZ	**LZ**, MZ		
LZ-CP	$La_2Zr_2O_7$	**LZ**, LA	**LZ**, LA	**LZ**, LA		

[a] Key: LA, La_2O_3; LZ, $La_2Zr_2O_7$; MZ, monoclinic ZrO_2; SZ, $SrZrO_3$; TZ, tetragonal ZrO_2; T, trace.

The sol−gel samples were obtained at nearly the nominal composition (cf. Table 1). The coprecipitated sample, however, contained more than 17 times more zirconium than strontium. An explanation for this observation may be the fact that strontium hydroxide is slightly soluble in aqueous ammonia, the precipitation medium used (Linke, 1965). It is therefore likely that the strontium cations were not incorporated to a large extent in the mixed hydroxide precipitate but remained in solution, yielding a composition far from target. Coprecipitation in a nonaqueous solvent may circumvent this problem.

The gel dried under supercritical conditions showed high crystallinity already at 1000 °C. Lowe *et al.* reported that crystallization already occurred during the supercritical drying step (Lowe *et al.*, 1995). The preparation of SZ-SG2 was an attempt to avoid this crystallization during drying. Probably, the crystallization of SZ-SG2 proceeded more slowly and in a more controlled manner than that of SZ-SG1. Hence, it is not unlikely that the SZ-SG2 consists of smaller crystallites than SZ-SG1, which could explain the difference in surface area. However, neither the $SrZrO_3$ peaks in the diffraction pattern nor SEM showed any significant differences between the two samples. A more detailed analysis of the diffraction patterns, with quantitative determination of the line broadening, would be needed to clarify this question.

$La_2Zr_2O_7$. Two lanthanum zirconate samples were prepared, one sol−gel sample (LZ-SG) dried at ambient conditions and one coprecipitation sample (LZ-CP) following route 2. The surface areas for the two samples after aging at various temperatures are given in Figure 7, and the observed crystalline phases are summarized in Table 2. Both materials had low surface areas, already after calcination at 1000 °C, at which temperature poorly crystalline materials were obtained.

After aging at 1100 and 1200 °C, the target pyrochlore phase appeared. The sol−gel sample contained zirconia impurities, which are probably related to the excess of zirconium in the material (cf. Table 1). The lanthanum ions may not have been incorporated in the gel during hydrolysis and polycondensation. The reason for this behavior is unclear at the moment, but it might be related to a too low hydrolysis ratio. The coprecipitated sample was obtained at a composition near target. The deviation from the target composition may be due to the uncertainty in the water content of the salts, in particular of the zirconium oxynitrate, in which case no specification of its water content was given by the supplier.

It is clear that the initial surface area of the $La_2Zr_2O_7$ will have to be improved by means of alternative synthesis routes if this material is to become of interest as a catalyst support.

Conclusions

A series of materials, reported as thermostable in literature, were prepared and subjected to aging in a stream of humid air. Such aging conditions are more representative for the conditions prevailing in catalytic combustors than thermal treatment in dry air. The thermal stabilities of some of the materials studied were in line with the expectations ($LaAl_{11}O_{18}$, $BaMnAl_{11}O_{19-\alpha}$), some showed disappointing behavior ($SrZrO_3$, $MgAl_2O_4$ (CP), $La_2Zr_2O_7$), and one material exhibited a higher thermal stability than anticipated ($MgAl_2O_4$ (SG)). Generally, sol−gel materials were superior to their coprecipitated counterparts; the most striking exception was $LaAl_{11}O_{18}$, showing similar thermal stability for the materials prepared by sol−gel synthesis and coprecipitation route 2. This coprecipitation route yielded more homogeneous materials than coprecipitation route 1, which proved to be beneficial for the thermal stability.

This work has been part of the on-going search for materials with improved thermal stability for catalytic combustion in gas turbine applications. Some indications are given by the obtained results. Clearly, the stoichiometry of the product is of great importance for both the thermal stability and the formation of desired and unwanted phases. Moreover, new synthesis methods may be applied advantageously, such as coprecipitation of materials other than hydroxides or in nonaqueous media.

These support materials will have to be used together with some kind of active phase, unless the active component is incorporated, which is the case for $BaMnAl_{11}O_{19-\alpha}$. Hence, the interaction between support and active phase and the influence of the active phase on support sintering will have to be taken into account. These issues have been studied for $LaAl_{11}O_{18}$-supported catalysts and have been presented separately (Zwinkels, 1996; Zwinkels *et al.*, 1996).

Acknowledgment

This work was supported by NUTEK, The Swedish National Board for Industrial and Technical Development. The authors wish to thank Inga Groth for valuable help with the XRD and BET analyses.

Literature Cited

Arai, H.; Yamada, T.; Eguchi, K.; Seiyama, T. Catalytic combustion of methane over various perovskite-type oxides. *Appl. Catal.* **1986**, *26*, 265.

Ashcroft, A. T.; Cheetham, A. K.; Green, M. L. H.; Grey, C. P.; Vernon, P. D. F. Oxidative coupling of methane over tin-containing rare-earth pyrochlores. *J. Chem. Soc., Chem. Commun.* **1989**, 1667.

Brinker, C. J.; Scherer, G. W. *Sol-gel science*; Academic Press: San Diego, 1990.

Dalla Betta, R. A.; Schlatter, J. C.; Chow, M.; Yee, D. K.; Shoji, T. Catalytic combustion technology to achieve ultra low NOx emissions: Catalyst design and performance characteristics. In *Proceedings of the 2nd International Workshop Catalytic Combustion*, 18−20 April, Tokyo; Arai, H., Ed.; Catalysis Society of Japan: Tokyo, 1994; p 154.

Furuya, T.; Yamanaka, S.; Hayata, T.; Koezuka, J.; Yoshine, T.; Ohkoshi, A. Hybrid catalytic combustion for stationary gas turbine - Concept and small scale test results. *ASME Paper 87-GT-99*, 1987.

Groppi, G.; Bellotto, M.; Cristiani, C.; Forzatti, P.; Villa, P. L. Preparation and characterization of hexaaluminate-based materials for catalytic combustion. *Appl. Catal. A* **1993**, *104*, 101.

Groppi, G.; Assandri, F.; Bellotto, M.; Cristiani, C.; Forzatti, P. The crystal structure of Ba-β-alumina materials for high-temperature catalytic combustion. *J. Solid. State Chem.* **1995**, *114*, 326.

Johansson, M.; McCarty, J.; Järås, S. G. Influence of oxygen pressure on methane combustion over $LaAlO_3$ supported transition metal oxides. 1996, submitted for publication.

Kato, A.; Yamashita, H.; Matsuda, S. Lanthanide β-alumina supports for catalytic combustion above 1000 °C. In *Successful design of catalysts*; Inui, T., Ed.; Elsevier: Amsterdam, 1988; p 32.

Kolaczkowski, S. T. Catalytic stationary gas turbine combustors: A review of the challenges faced to clear the next set of hurdles. *Trans. IChemE.* **1995**, *73*, 168.

Linke, W. F. *Solubilities of inorganic and metal-organic compounds*; American Chemical Society: Washington, DC, 1965.

Lowe, D. M.; Gusman, M. I.; McCarty, J. G. Synthesis and characterization of sintering resistant aerogel complex oxide powders. In *Preparation of Catalysts VI*; Poncelet, G., Jacobs, P. A., Grange, P., Delmon, B., Eds.; Elsevier Science B.V.: Amsterdam, 1995; p 445.

Machida, M.; Eguchi, K.; Arai, H. Effect of additives on the surface area of oxide supports for catalytic combustion. *J. Catal.* **1987**, *103*, 385.

Machida, M.; Eguchi, K.; Arai, H. Preparation and characterization of large surface area $BaO.6Al_2O_3$. *Bull. Chem. Soc. Jpn.* **1988**, *61*, 3659.

Machida, M.; Eguchi, K.; Arai, H. Catalytic properties of Ba $MAl_{11}O_{19-\alpha}$ (M = Cr, Mn, Fe, Co, and Ni) for high-temperature catalytic combustion. *J. Catal.* **1989**, *120*, 377.

Marion, M. C.; Garbowski, E.; Primet, M. Catalytic properties of copper oxide supported on zinc aluminate in methane combustion. *J. Chem. Soc., Faraday Trans.* **1991**, *87*, 1795.

Marti, P. E.; Maciejewski, M.; Baiker, A. Methane combustion over $La_{0.8}Sr_{0.2}MnO_{3+x}$ supported on MAl_2O_4 (M=Mg, Ni and Co) spinels. *Appl. Catal. B* **1994**, *4*, 225.

Marti, P. E.; Maciejewski, M.; Baiker, A. Methane combustion over $La_{0.8}Sr_{0.2}MnO_{3+x}$ supported on $LaAlO_3$ and $LaAl_{11}O_{18}$ prepared by different methods: Influence of preparation method on morphological and catalytic properties in methane combustion. In *Preparation of Catalysts VI*; Poncelet, G., Jacobs, P. A., Grange, P., Delmon, B., Eds.; Elsevier Science B.V.: Amsterdam, 1995; p 617.

McCarty, J. G.; Wise, H. Perovskite catalysts for methane combustion. *Catal. Today* **1990**, *8*, 231.

Prasad, R.; Kennedy, L. A.; Ruckenstein, E. Catalytic Combustion. *Catal. Rev. Sci. Eng.* **1984**, *26*, 1.

Ramesh, K. S.; Cox, J. L.; Parks, W. P. J. Materials for high temperature catalytic combustion. In *Proceedings of the 2nd International Workshop Catalytic Combustion*, 18−20 April, Tokyo; Arai, H., Ed.; Catalysis Society of Japan: Tokyo, 1994; p 42.

Sadamori, H.; Tanioka, T.; Matsuhisa, T. Development of a high temperature combustion catalyst system and prototype catalytic combustor turbine test results. In *Proceedings of the Second International Workshop Catalytic Combustion*, 18−20 April, Tokyo; Arai, H., Ed.; Catalysis Society of Japan: Tokyo, 1994; p 158.

Trimm, D. L. Thermal stability of catalyst supports. In *Catalyst Deactivation V*; Bartholomew, C. H., Butt, J. B., Eds.; Elsevier: Amsterdam, 1991; p 29.

Zwinkels, M. F. M. High-temperature catalytic combustion. Ph.D. Dissertation, Royal Institute of Technology: Stockholm, Sweden, 1996.

Zwinkels, M. F. M.; Järås, S. G.; Menon, P. G.; Griffin, T. A. Catalytic materials for high-temperature catalytic combustion. *Catal. Rev. Sci. Eng.* **1993**, *35*, 319.

Zwinkels, M. F. M.; Järås, S. G.; Menon, P. G. Preparation of combustion catalysts by washcoating alumina whiskers-covered metal monoliths using a sol-gel method. In *Preparation of Catalysts VI*; Poncelet, G., Jacobs, P. A., Grange, P., Delmon, B., Eds.; Elsevier Science B.V.: Amsterdam, 1995; p 85.

Zwinkels, M. F. M.; Haussner, O.; Menon, P. G.; Järås, S. G. Preparation and characterization of $LaCrO_3$ and Cr_2O_3 methane combustion catalysts supported on $LaAl_{11}O_{18}$- and Al_2O_3-coated ceramic monoliths. 3rd Workshop on Catalytic Combustion, 23−25 September, 1996, Amsterdam; to be published in *Catal. Today*.

Received for review July 19, 1996
Revised manuscript received October 20, 1997
Accepted October 27, 1997[⊗]

IE960421I

[⊗] Abstract published in *Advance ACS Abstracts*, December 15, 1997.